Dynamic Simulations Show Repeated Narrowing Maximizes DNA Linearization in Elastomeric Nanochannels

Minsub Han[1*], Byoung Choul Kim[2,3,4], Toshiki Matsuoka[2,4], M.D. Thouless[5,6] and Shuichi Takayama[2,3,4,7,8]

[1] Department of Mechanical Engineering, College of Engineering, Incheon National University, Songdo-dong, Yeonsu-gu, Incheon, Korea 406-772

[2]Department of Biomedical Engineering, College of Engineering, University of Michigan, 2200 Bonisteel Blvd, Ann Arbor, MI 48109, USA

[3]Macromolecular Science and Engineering Center, College of Engineering, University of Michigan, 2300 Hayward St., Ann Arbor, MI 48109, USA

[4]Biointerfaces institute, University of Michigan, 2800 Plymouth Rd, Ann Arbor, MI 48109, USA

[5]Department of Mechanical Engineering, College of Engineering, University of Michigan, 2350 Hayward St., Ann Arbor, MI 48109, USA

[6]Department of Materials Science & Engineering, College of Engineering, University of Michigan, 2300 Hayward St., Ann Arbor, MI 48109, USA

[7]Michigan Center for Integrative Research in Critical Care, University of Michigan, Ann Arbor, MI 48109, USA

[8]Division of Nano-Bio and Chemical Engineering WCU Project, UNIST, Ulsan, Republic of Korea

*author to whom correspondence should be addressed.

Abstract

This paper uses computer simulations to reveal unprecedented details about linearization of DNA inside dynamic nanochannels that can be repeatedly widened and narrowed. We first analyze the effect of rate of channel narrowing on DNA linearization dynamics. Quick (~0.1s) narrowing of nanoscale channels results in rapid overstretching of the semi-flexible chain followed by a slower (~0.1-10s) relaxation to an equilibrium extension. Two phenomena that induce linearization during channel narrowing, namely elongational-flow and confinement, occur simultaneously, regardless of narrowing speed. Interestingly, although elongational flow is a minimum at the mid-point of the channel, and increases towards the two ends, neither the linearization dynamics nor the degree of DNA extension vary significantly with the center-of-mass of the polymer projected on the channel axis. We also noticed that there was a significant difference in time to reach the equilibrium length, as well as the degree of DNA linearization at short times, depending on the initial conformation of the biopolymer. Based on these observations, we tested a novel linearization protocol where the channels are narrowed and widened repeatedly, allowing DNA to explore multiple conformations. Repeated narrowing and widening, something uniquely enabled by the elastomeric nanochannels, significantly decreases the time to reach the equilibrium-level of stretch when performed within periods comparable to the chain relaxation time and more effectively untangle chains into more linearized biopolymers.

I. Introduction

Deoxyribonucleic acid (DNA) is the bio-molecular storage medium of genetic information for living organisms. DNA is a linear polymer whose size is extremely disproportionate in that the ratio of its length to width is on the order of 10^9 in human cells. DNA in the nucleus therefore exists in highly compact and condensed structures. Even purified and decondensed DNA *in vitro* forms a globular and coiled structure in solution. However, a number of analysis techniques, such as DNA mapping [1-3], require DNA chains to be linear, rather than coiled.

There are a number of mature techniques to linearize DNA, which have been reviewed extensively in recent papers [4-8]. An early method to stretch DNA was to tether each end of the molecule to a bead, and to apply an extensional force using optical or magnetic tweezers [9]. Later, various flow-based stretching methods were investigated [5]. These usually relied on applying a moving boundary, a pressure gradient, or an external electrical field. The resultant flows induced by these driving forces tend to be simple shear, cross, or converging flows that all result in extensional-strain distributions.

Recently, confinement of linear polymers in one or two dimensions has attracted attention as an effective tool to linearize them [6, 10-16]. Nanoscale slits or channels can drastically reduce the degree of freedom of DNA and induce linear conformations. More recently, a method to linearize DNA using squeezing flows generated inside elastomeric nanochannels was reported (Fig. 1) [17]. The method uses tunneling cracks generated in an elastomer whose channel dimensions can be adjusted by applied strain [18, 19]. Two features of this method stand out from the other methods described in the literature. One is that the geometry

of the channels is not fixed, and is easily tunable. Another is that effects of both flow and confinement are used together, leading to effective linearization of linear bio-polymers under low-shear-stress conditions. This method will therefore improve the mature technologies involving DNA linearization [20, 21]. However, while nearly full-linearization of DNA and chromatin has been demonstrated, variables in the procedure are yet to be fully understood and controlled.

The aim of the present study is to enhance the understanding of the physical processes behind the method, and to build a knowledge base upon which efficient and reliable experimental protocols can be developed. There are, however, a number of non-trivial modeling tasks required to simulate squeezing-flow-mediated DNA linearization. For example, the flow is strongly transient in the initial phase of the squeezing process. Because there are significant three-dimensional elongational flows, as well as potential hydrodynamic effects between the chain components, the solvent is better modeled explicitly. In addition, because the length scales and the configurational regimes in the problem are quite varied, no existing single modeling approach can cover the entire process from the globular state to the fully-linearized state of the DNA. Here, we focus on the dynamic processes occurring during the early stages of channel narrowing and DNA linearization, where the channel starts out relatively wide and then narrows down to a few persistence lengths in width. DNA is modeled as a semi-flexible polymer, using the bead-spring model of Underhill and Doyle [22]. Furthermore, we use a particle-based mesoscale-modeling method called the dissipative-particle-dynamics (DPD) technique to model the solvent [23]. The flow condition within a narrowing curved wall is modeled by adopting an image-particle-based technique [24, 25], and the condition at the exit is modeled by using selective deletion proportional to the velocity profile. In all, the

integrated modeling approach ensures that the DNA linearization in squeezing flow is accurately simulated with modest computational cost.

We analyze the basic features of DNA extension during the process of narrowing the nanochannel, focusing on the effects of elongational flows and confinement effects. We also investigate how simple differences in the sample, and practical changes in the narrowing procedures, might significantly affect the outcomes. More specifically, we consider the effects of chain length, initial degree of extension, and squeeze-relax-squeeze operations on the process.

II. Simulation Method

The experimental procedure that we are simulating is referred to as "nanoscale squeezing." It starts with the application of tensile strains to an elastomeric bulk substrate that has normally-closed nanochannels constructed within it. Super-resolution microscopy measurements indicate that a strain of about 10% on the substrate causes the normally-closed channels to open to about 750nm in width. The open channels are then filled with DNA solution (the experiments used DNA from λ-phage, which we will refer to as λ-DNA). When the applied strain is completely released, the fluid is squeezed out, and the channels fully relax in less than a few seconds. The equilibrium state of a λ-DNA chain confined within a narrow channel can be estimated from previously published results [26, 27]. This literature suggests that, if the cross-sectional diameter of a circular channel, D, is greater than 1500 nm, the λ-DNA is in its bulk state. If the diameter is in the range 600 nm < D <1500 nm, then the de Genes regime applies. If the diameter is in the range 100 nm < D < 600 nm, then the extended de Genes regime applies. If the diameter is less than 50 nm, the Odijk regime applies, with a cross-over regime exiting in the range of 50 nm < D < 100 nm.

Experimentally, the most significant change in the degree of linearization occurs in the early stages of the squeezing process, when the channel is larger than the persistence length. This corresponds to the de Gennes and the extended de Gennes regimes, in which both flow-mediated elongation and confinement effects are important. On the other hand, confinement effects will dominate in the Odijk regime. Our simulations, therefore, focus on the dynamic process occurring during the early stages of channel narrowing and DNA linearization. This contrast with the linearization by confinement without flow where the biggest slope in the extension versus channel size is in the cross-over regime [28].

This manuscript was accepted by Biomicrofluidics. Click here to see the version of record.

The simulation model consists of four basic components: elastic channel, DNA, solvent, and channel-solution interaction. First, the governing equation for the narrowing of liquid-filled elastic channels is solved to obtain the radial boundary condition as a function of time. We consider the relatively simple geometrical case of a circular tube widened under axisymmetric strain applied on the outer walls. When the applied strain is released, the tube starts to narrow from the tube ends. The geometry is simpler here than that in the model experiment [17] where a channel of a large aspect ratio is under uniaxial strain. The effect of the difference would not be trivial [29-31] but is not pursued further in this work. The evolution of the tube inner radius is governed by the following equations [29]:

$$\frac{\partial R_i}{\partial t} = \frac{ER_{io}^2}{24\mu}\frac{\rho_o^2-1}{\rho_o^2}\frac{\partial^2 R_i}{\partial \mathrm{x}^2} \tag{1}$$

with

$$R_i(\mathrm{x},0) = R_{io}; R_i(\pm \mathrm{x}_{max}, t) = R_{ie} \tag{2}$$

where R_i is the local inner radius of the tube, R_{io} is the initial inner radius before strain release, R_{ie} is the final inner radius after complete narrowing of the tube after the strain is released, ρ_o is the ratio of the initial outer radius to the initial inner radius. E is the Young's modulus, μ is the liquid viscosity, and z is the axial coordinate. The tube ends are located at $\mathrm{x} = \pm \mathrm{x}_{max}$, respectively. The fluid flow is modeled as Poiseuille flow in the limit of narrow

tubes, and the velocity profile is given as

$$u_x = \frac{E}{6\mu R_{io}} \frac{\rho_o^2 - 1}{\rho_o^2} \frac{\partial R_i}{\partial \mathrm{x}} (R_i^2 - r^2), \quad (3)$$

The term $\frac{\partial R_i}{\partial z}$, along with R_i, varies with x and imparts the axial dependence of the flow field. Equation (3) is the velocity distribution that is not perturbed by the DNA chain in the collapsing channel, and will be the basis for the boundary conditions of DPD at the axial ends. We chose initial conditions to match values from experiments. The initial inner radius is chosen as $R_{io} = 0.75\mu m$, which is the channel width under 10% strain as determined from super-resolution microscopy [32]. In a normal experiment, the strain is released not at one go, but with multiple steps for gentler linearization. Because we also focus on the early stages of channel narrowing, we set the final inner radius in the simulation as R_{ie} = 0.43 μm, which is within the range of the extended de Gennes regime. Equation (1) is in a form of diffusion equation with a constant $C \equiv (ER_{io}^2/24\mu)(\rho_o^2 - 1)/\rho_o^2 [\mu m^2/s]$ that is a measure of the spreading speed of collapsing front. For reference, dimensioned parameters that give a value of C = 10^6 [μm^2/s] are an outer radius of 1000[μm], a solvent viscosity of 0.001[kg/(m·s)], and E = 4.27x10^4 [kg/(m·s^2)]. The shear rate and strain rate developed by the channel are estimated to be about 85.2 and 73.2 [1/s], respectively (See Appendix I).

Next, the DNA, a semi-flexible linear polymer, is modeled in the simulation as beads connected with extensional non-linear springs. The spring model by Underhill and Doyle [33] is used. The spring force between the beads is:

This manuscript was accepted by Biomicrofluidics. Click here to see the version of record.

$$f_s(r) = \frac{k_B T}{l_p}\left\{\frac{\hat{r}}{(1-\hat{r}^2)^2} - \frac{7\hat{r}}{v(1-\hat{r}^2)^2} + \left(\frac{2}{32} - \frac{3}{4v} - \frac{6}{v^2}\right)\hat{r} + \left(\frac{\frac{13}{32}+\frac{0.8172}{v}-14.79/v^2}{1-\frac{4.225}{v}+4.87/v^2}\right)\hat{r}(1-\hat{r}^2)\right\}, \quad (4)$$

where r is the distance between interacting particle centers, $v = l_{max}/l_p$ and $\hat{r} = r/l_{max}$. l_{max} is the maximum extensible length of the spring. l_p is the persistence length. k_B is the Boltzmann constant. T is the absolute temperature. This bead-spring chain model is a coarse-grain model of the continuous worm-like-chain; it is reported to be reliable for long polymers in both the small and large extension limits [33, 34]. The spring in the model can also represent dimensions as small as two persistence lengths, which is consistent with our simulations, where the smallest channel size is comparable to the persistence length.

In a dilute polymer solution, it is important to consider the hydrodynamic interaction through which one segment of a polymer can influence another, even if they are far apart in the sequential order along the molecule. In addition, the polymer is actively acted upon by the squeezing flow that is established within the solvent in response to the wall movement. To include these influences effectively, it is useful to model the solvent explicitly using a coarse-grained model based on dissipative particle dynamics [23]. The dissipative particles represent an average effect of a large number of molecules. The collective behaviors of the particles simulates the behavior of molecules at a much coarser scales and, thus, at a lower computational cost. The equations of motions in dissipative-particle dynamics (DPD) are

$$\frac{d\vec{r}_i}{dt} = \vec{v}_i \ , \quad (5)$$

This manuscript was accepted by Biomicrofluidics. Click here to see the version of record.

$$\frac{d\vec{v}_i}{dt} = \vec{F}_i = \sum_j \vec{F}_{ij}^C + \vec{F}_{ij}^D + \vec{F}_{ij}^R. \quad (6)$$

$\vec{r}$ and $\vec{v}$ are the particle position and velocity vectors, respectively, and the subscripts i, j are the particle numbers. $\vec{F}_{ij}$ is the force between two interacting particles with the conservative, dissipative, and random forces being indicated with the superscripts *C*, *D*, and *R*, respectively.

$$\vec{F}_{ij}^C = \begin{cases} a_{ij}(1 - r_{ij})\hat{r}_{ij}, & r_{ij} < r_C \\ 0, & r_{ij} \geq r_C \end{cases}, \quad (7)$$

$$\vec{F}_{ij}^D = -\gamma\omega^D(r_{ij})(\hat{r}_{ij} \cdot \vec{v}_{ij})\hat{r}_{ij}, \quad (8)$$

$$\vec{F}_{ij}^R = \sigma\omega^R(r_{ij})\zeta_{ij}\hat{r}_{ij}, \quad (9)$$

where,

$$\vec{r}_{ij} = \vec{r}_i - \vec{r}_j;\ r_{ij} = |\vec{r}_{ij}|;\ \hat{r}_{ij} = \vec{r}_{ij} / r_{ij},$$

and r_c is the cutoff radius for the interaction. As will be elaborated later, r_c is the basic unit of DPD simulation and set as twice the persistence length of DNA so that all the other length scales are based on r_c or $2l_p$. In these equations, ζ_{ij} is a Gaussian white noise function with symmetry, $\zeta_{ij} = \zeta_{ji}$, to ensure the momentum conservation and satisfies the following stochastic properties:

$$\langle\zeta_{ij}(t)\rangle = 0; \langle\zeta_{ij}(t)\zeta_{kl}(t')\rangle = (\delta_{ik}\delta_{jl} + \delta_{il}\delta_{jk})\delta(t - t'). \quad (10)$$

This manuscript was accepted by Biomicrofluidics. Click here to see the version of record.

The fluctuation-dissipation relationship gives

$$\sigma^2 = 2k_B T\gamma, \tag{11}$$

and

$$\omega^D(r) = [\omega^R(r)]^2 = \begin{cases} (1 - r/r_C)^S, & r < r_C \\ 0, & r \geq r_C \end{cases} . \tag{12}$$

All the parameters and functions except for ρ_n and s, defined below, are given according to the original DPD prescription by Groot and Warren [23]. The values of a_{ij} of the non-bonded conservative force are given by

$$a_{ij} = 75k_B T/\rho_n, \tag{13}$$

where ρ_n is the number density of the solution, including both the solvent and DNA particles. The values of a_{ij} were derived by matching the compressibility of water, based on the equation of state of a DPD fluid. This is used for all the non-bonded interactions between solvent particles and beads in the chain. $\sigma = 3$ is used as a random-force coefficient, which was recommended in terms of stability and performance in the dissipation. Equation (11) then gives $\gamma = 4.5$. While the original choice in [23] is $\rho_n = 3/r_c^3$ and $s = 2$, we set the density and exponent as $\rho_n = 4/r_c^3$ and $s = 1/2$, respectively. These values give a higher rate of collisions and, thus, higher viscous dissipation, improving the ability to model the viscosity of water [35].

In this DPD representation of DNA solution, the beads in the DNA chain and solvent are of

the same size and under the same interaction-forces of Eqs. (7-9), constituting an athermal solvent, while the beads in the chain are under the additional spring force of Eq. (4). The simulated chain dynamics in equilibrium agrees well with the Zimm model for a chain in good solvent [36]. The hydrodynamic interactions between the segments of the chain are then well represented. So are the interactions between the chain segment and the wall by introducing $s = 1/2$ in Eq. (12) [37]. It also turns out that additional force is not necessary for enforcing excluded volume interaction between DNA chain segments. The repulsive force of Eq. (7), while soft, is enough for simulating the chain with excluded volume interaction under less than extremely high temperature [36].

Because fluid-solid interfaces confine the DNA and drive the fluid flow, it is essential to apply accurate boundary conditions. Three types of boundary conditions must be satisfied at the surfaces of the channels, which are assumed to be cylindrical in this simulation. First, the no-penetration condition is applied by a straightforward method in which any particle that crosses the boundary in the simulation is, instead, specularly reflected. Second, the no-slip condition is obtained by distributing mirror-image particles outside the boundary; these have an opposite axial velocity to the original particles and interact with the same DPD forces [24, 38]. Third, the motion of the wall during the collapse of the channels is prescribed by as a function of time. This time history of the wall position is obtained by solving the Eq. (1), as described before. An alternative way to prescribe the wall motion is to apply a pressure on the cylinder surface. However, the pressure in the simulation fluctuates considerably, so displacement-controlled boundary conditions are used.

The boundary conditions at the exits require special modeling. The axial length of a typical

nanochannel (~300μm) is far larger than the radius (~1μm-50nm), so it is radial confinement that dominates the DNA dynamics. Even fully-linearized λ-DNA, which has a contour length of about 22 μm, occupies only a small fraction of the axial length of the channel. The rest of the channel volume is composed of solvent molecules that have only an indirect influence on the DNA, but would require the major part of the computation if they were directly modeled. Therefore, we conduct the simulation over a shorter axial domain, with a boundary condition assuming fully-developed flow at the ends of the domains. The boundary regions at these ends have a length of $2.5r_c$ (see Fig. 2a). The particles in the regions become the candidates for deletion whenever the particle number in the region exceeds the equilibrium number. It can be mentioned that, in a real experiment, a situation can typically arise where multiple of DNA occupy a channel, for example, for high throughput genome mapping [39].

We devised a simple method to apply the required velocity profile on the end boundaries: each solvent particle is selected randomly in the deletion operation, but the probability of the selection is weighted according to the parabolic velocity profile of the fully-developed flow. The average density of the system is then controlled to be approximately constant when the volume decreases during the squeezing process. Whenever a portion of the DNA enters the boundary region, the simulation is repeated with a larger initial volume. Most of the results in this study concern the squeezing process, but a reverse, relaxing-back, process is also considered later in the context of a periodic squeeze-relax process. At the boundaries, to keep the system density constant, the particles are inserted similarly at the selected positions proportional to parabolic profile. Because the particle interaction potential is of soft nature, the particle overlap is not a major concern in selecting the insertion position as in the molecular dynamics. The resultant compact domain size makes the computational load less

demanding. More comprehensive multiscale approaches combining a continuum solver and particle simulation are available, but are not pursued here because this simple passive condition appears to be sufficient [40].

To make the model of the DNA chains and water representative of the experimental system, we first set the basic scales of the simulation to be consistent with those of the experiments. Energy is normalized by k_BT in the simulation. Therefore, the temperature is set to 1, recognizing that this corresponds to a dimensioned value of $[k_BT]/k_B$. The cut-off length, r_c, which is the basic length in DPD, is set equal to $2l_p$. The maximum bond length is set as $5l_p$. The λ-DNA is assumed to have a contour length of 22 μm and a persistence length of 53 nm. The third basic dimension in DPD simulations is usually chosen to be that of the mass of the solvent. However, this results in a viscosity that is far less than that of water because the soft interaction potential generally used in DPD models [23] results in less dissipation within the fluid than occurs within real liquids [35]. In our model system, the transfer of matter by the flow in the channel is a critical element in assessing the linearization dynamics of DNA. Therefore, the viscosity in the DPD simulation is chosen to match that of water. The time unit in the simulation is then [3.61×10^{-5}s]. The inevitable consequence of this choice is that the density of the solvent is much larger than that of water, so the speed of sound is lower than it is in water. This imposes an upper bound on the wall speed required to keep the solvent approximately incompressible.

On the modeling side, we first validated the basic simulation code in three ways. Two of the validations involved consideration of static configurations: one in the bulk state, and the other in a confined state. In the former case, polymer chains of various contour lengths were put

This manuscript was accepted by Biomicrofluidics. Click here to see the version of record.

into a cylinder of 4 μm in length and diameter. The radii of gyration resulting from the simulations were compared to experimental results available in the literature [41], as shown in Fig. 2(b). We next considered the configuration of chains confined in narrow tubes. There are few relevant experimental data on DNA linearization in channels of similar geometry and size in the literature. Therefore, we compared the simulation results with separate theoretical predictions based on analyses in the de Gennes regime (Fig. 2(c)). The contour length of DNA is 22μm. The following relationship between the mean extension and channel diameter was used:

$$\langle X \rangle / L = C_o D^{(\nu-1)/\nu}, \tag{14}$$

where $\nu = 0.5877$, as recommended in [28], and $C_o = 9.72$ were used to generate the results shown in Fig. 2(c). Both sets of comparisons show reasonable agreements. The disagreement in the smallest tube diameter in Fig. 2(c) is likely to indicate lack of sufficient resolution rather than transition to the crossover regime. The tube diameter there is less than twice the bead diameter while it is about the border between the extended de Gennes and crossover regimes [28]. The parameters in the fitting can be compared with those in $\langle X \rangle / L \cong 24.7 D^{-0.86}$ of [42], which covers extended de Gennes and crossover regimes. Finally, we examined whether the simulation can produce a correct profile of the axial flow in the channel. When the tube diameter was much greater than the size of the beads, a fully-developed flow corresponding to the expected Poiseuille flow was obtained after applying an axial body force on the solvent (Fig. 2(d)). When the ratio of the tube diameter to the bead size was less than about 2, the flow deviated from Poiseuille flow. When the size of the bead becomes comparable to that of the tube, the particulate feature of the beads became

noticeable near the wall, and the solvent became less homogeneous. This, along with the results in Fig. 2(c), puts a lower limit of about 3 on the tube diameter with respect to the bead size in the simulation. This limit corresponds to 6 times the persistence length of DNA in our simulation. Therefore, the bulk and blob regimes, de Gennes and extended de Gennes, are within the capability of our simulation study.

III. Simulation results

In the following results, we describe the state of the DNA chain mainly in terms of the extension. There are several different measures of the extension that can be used: the end-to-end distance, the chain span along the channel axial direction, and the radius of gyration are examples. We chose the chain span in the channel axial direction, X, which is often used in related literature because it is easier to measure in experiments. Many simulation results presented are time trajectories of the axial chain span where the mean axial span, $\langle X \rangle$, implies ensemble-averaged data. In the ensemble average, several trajectories for the same boundary conditions, including the initial and boundary conditions, are averaged for the same given time.

III-1. Single squeeze operation: We first consider single-squeeze results, in which the channel diameter changes in response to a single decrement of strain. The governing equation for collapsing channel (Eq.(1)) was numerically solved using the finite difference method with R_{ie} = 0.43 μm and a half-channel length of z_{max} = 150μm (See Appendix II). In Fig. 3(a), the change in the channel diameter with time at z=0 is shown for four collapsing channels with collapse constants in the range of $C = 10^4$ to 10^7 [μm^2/s]. For example, the diameter of a tube containing the DNA solution decreases from 750 nm to 430 nm in about 1 sec for

This manuscript was accepted by Biomicrofluidics. Click here to see the version of record.

C=10^5[μm^2/s] and in about 0.1 sec for C=10^6[μm^2/s], respectively, according to the solution of Eq. (1). This can be compared with the experimental observations that the rate of the nanochannel squeeze is comparable to a second [17]. In Fig. 3b, two DNA linearization results are shown according to the collapse constants of C=10^5[μm^2/s] and C=10^6[μm^2/s], respectively. The time history of the mean axial span is obtained by ensemble averaging over 10 trajectories. The squeezing flow in the narrowing nanochannel induces the linearization of the DNA by two distinct processes. First, the DNA chain is over-stretched in a short period of time by the strong elongational flow. It next relaxes back slowly to a new equilibrium state with the newly-narrowed confinement. The latter process can, therefore, be characterized as the confinement effect. The former can be characterized as the elongational-flow effect. After a sufficiently long time, the final degree of linearization would depend only on the degree of confinement. However, the path and time to reach the equilibrium state depend on both the effects.

The axial distribution of the monomers clearly shows the process of over-extension and relaxation back to the confined state (Fig. 3(c)). During the long relaxation period, the monomers become more evenly distributed. The radial distribution of monomers initially shows a rather monotonic decrease from the centerline towards the tube wall (Fig. 3(d)). In Fig. 3(c,d), the distributions are obtained by centering the center-of-mass and ensemble-averaging 37 trajectories. The monomers are then concentrated toward the centerline right after the squeezing period and slowly relax back to the more monotonic distribution with time.

III-2. Effect of initial conditions on extension: We next investigate the extension dependence on the initial conditions such as the extension and the center-of-mass (CM) position in the

This manuscript was accepted by Biomicrofluidics. Click here to see the version of record.

channel axis of chains at the start of the squeeze. The axial CM position of the DNA in a channel varies in a typical experimental setting, owing to thermal fluctuations, as does the initial extension to a lesser degree. We first set up the DNA in various axial CM positions and compared the maximum extensions induced by squeezing. The axial CM positions are determined by the average of bead x-coordinates. Fig. 4(a) shows the dependence on the axial CM position at the start of the squeeze. Because any chain whose CM is initially in a positive x-coordinate is under the same physical condition as the chain in a negative x-coordinate of the same absolute value and the outcome will be the same on average, only the chains whose CM is located in a positive x-coordinate is considered. It turns out that the axial-CM-position variation does not affect the degree of extension significantly even at the short times. In a squeezing flow, the strain rate $\dot{\varepsilon}$ is highest at the centerline and is constant with respect to the axial CM position, while the shear rate of $|\dot{\gamma}|$ increases with distance away from the center of the tube, in both the radial and axial directions. The relatively low dependence on axial CM position suggests that, although chains in different locations in the channel axis may undergo different shear rates, the chain is distributed mostly around the centerline, where the effect of the shear is always low. On the other hand, it is clear that the maximum extension is positively correlated with the extent of the initial channel-axial extension for the same data (square symbols in Fig. 4(b)).

This dependence of the extent of linearization on the initial extension may also explain other phenomena. Figure 4(c) shows the single-squeeze results of chains of various contour lengths. The degree of over-extension and recoiling time increases with contour length. The recoiling time must increase, because the extended length for the recoiling increases with the span of the chain in the channel-axial direction. However, the maximum extension ratio, represented

This manuscript was accepted by Biomicrofluidics. Click here to see the version of record.

by $<X_{max}>/L$, is a relative parameter, and would not increase with contour length if the initial extension ratio were the same. As we discussed, the elongational flow near the centerline gives the most dominant effect on linearization, and the centerline strain rate is constant in the axial direction. A more plausible explanation is that a longer chain under the same confinement conditions would have a larger (initial) extension ratio, which leads to a larger maximum extension (See solid circles in Fig. 4(b)). In other words, the initial chain configurations that give the DNA a more ellipsoidal, rather than spherical, shape overall, are more effectively stretched by elongational flows. This indicates that the squeezing method is very effective in linearizing longer chains, and that the longer chains need a smaller strain change, or a longer relaxation period, to prevent cleavage.

III-3. Periodic-squeeze operation: In experiments, some DNA ends up in tangled states that make further linearization difficult [10]. Based on the afore-described characteristics of chain dynamics in squeezing flow, use of repeated application of strain was simulated to investigate the ability of the procedure to alleviate such tangled states. Three distinctive chain distributions were prepared, and their responses to the application of a periodic strain were studied (Fig. 5(a)). These were the globular, dumbbell, and half-dumbbell configurations. In Fig. 5, the numbers associated with the identification of the configurations indicates the fraction of the chain in the linear form (See also Appendix III). The cross-sectional profile was imposed by repeated application of a squeeze-relax-squeeze-relax operation in which the diameter changed between 629.3 nm and 449.5 nm over periods varying between 0.07 and 1.06 seconds (see the inset in Fig. 5(b)). Four evolution trajectories are ensemble-averaged in Fig. 5(b-e). Most of the profiles simulate gentle periodic squeeze-relax operation that should be possible to realize experimentally.

When the period of the squeeze-relax-squeeze operation is sufficiently large, the DNA conformation approaches an equilibrium state, well before the next cycle. The response of the DNA is then periodic, following the imposed operation. However, the period of the squeezing procedures can be made to not allow the chains to reach complete equilibrium (Fig. 5(b)). When the period of the squeeze is sufficiently smaller than the relaxation time of the chain, repeated squeezes linearize more effectively, even though the final tube diameter and degree of confinement are the same for all cases. The relaxation time of DNA can range from 0.64 s, based on a rough fit of the data in [12], to as short as 0.07 s. (Fig. 5(c-e)). The dumbbell-like distribution benefited most from repeated squeeze-relax operations because it is in the most linearized state to begin with in terms of having large *X/L* values and small globular fractions. Also, in some cases, the standard deviation grows rapidly in time when a chain among the ensemble is linearized much faster than the rest. The dumbbell-like distribution is linearized more consistently than the half-dumbbell whose ensemble shows large deviations at later times. More quantitative analysis may be possible by comparing the responses of different configurations according to a single squeeze. For the purpose, the period of the operation is set sufficiently long, $T_{interval}$=4(sec). In Table I, dumbbell 0.1 and half-dumbbell configurations have larger initial degree of extention, $< X >_{initial}/L$, than the rest. This leads to higher maximum extensions. Furthermore, of the two configurations, the dumbbell 0.1 has longer relaxation time. The difference is likely to come from the hydrodynamic drag the fractions of the chain overcome to recoil back. The two fractions of globular sub-configurations at both ends in a dumbbell configuration may face larger drag than the region of linear sub-configuration in a half-dumbbell configuration. These points again underscore the fact that the initial degree of linearization is one of the most dominant factors that

determine final linearization result.

IV. Conclusion

This work uses computer simulations to provide a deeper mechanistic understanding of a previously published experimental method that uses cross-sectional size-adjustable nanochannels to effectively linearized biopolymer chains such as DNA and chromatin. The mesoscale simulations were performed using a dissipative-particle-dynamics method that allows analysis of DNA linearization by both squeezing-induced hydrodynamic flow as well as by confinement in elastomeric nanoscale channels. The model specifically targeted the configurational change from the de Gennes regime to extended de Gennes regime, and the solvent was modeled explicitly. Semi-flexible chain dynamics were modeled by the bead-spring model of Underhill and Doyle, and the characteristic time for the squeezing rate was obtained by solving the governing equations for axisymmetric collapse of liquid-filled elastic channels. The insights obtained not only explain previous experiments but additionally point to new experimental procedures that may further enhance biopolymer linearization in these systems through the use of optimized sequential and repeated nanoscale squeezing procedures.

The major findings from the simulation are summarized as follows.

1. Squeezing DNA solutions in nanoscale channels causes a quick initial overstretching of the chain followed by a far slower relaxation of the chain to its equilibrium state in the newly narrowed channel. The dual existence of the initial elongational flow and the subsequent confinement effects makes the process effective in linearizing biopolymers.

2. A larger degree of initial extension positively affects the linearization performance. On the other hand, there was no noticeable influence of the initial CM position of the

chain. The latter fact suggests that the hydrodynamic flow effect mainly comes from the elongation near the centerline, rather than from the shear flow near the walls. A chain with a larger contour length is more effectively linearized by a given channel and squeezing procedure because the initial degree of extension will be larger.

3. A periodically repeated application of squeeze-and-expand was helpful in linearization. It was found that, if the applied period is in the same order as that of the relaxation time of the chain, repeated channel narrowing rewidening and renarrowing may be helpful in gently unraveling the chain from an entangled state.

Although our model analyzes cylindrical channels which are different from the more diamond-shaped cross-sectional shape of experimentally utilized channels, we believe that the essential physical features and biopolymer linearization characteristics are shared by both geometries. The effect of geometrical shape on linearization performance also has practical importance and deserves further study. Other outstanding topics of future study are the chain dynamics in the cross-over and Odijk regimes, the linearization of polymers more structured than DNA such as chromatin, and experimental testing of new procedures suggested by the simulation studies.

This manuscript was accepted by Biomicrofluidics. Click here to see the version of record.

Appendix I: shear and strain rates in collapsing channel

Based on the solution of Eq. (1) and (2) with Eq. (3), the shear rate and strain rate in the collapsing channel can be expressed, respectively, as

$$\epsilon_{rx}(\mathrm{r},\mathrm{x},t) = \left(\frac{\partial u_r}{\partial x} + \frac{\partial u_x}{\partial r}\right) = -C\,\frac{4}{R_{io}^3}\frac{\partial R_i}{\partial x}r, \tag{A.3}$$

$$\epsilon_{xx}(\mathrm{r},\mathrm{x},t) = \left(\frac{\partial u_r}{\partial r} + \frac{\partial u_x}{\partial x}\right) = -C\,\frac{4}{R_{io}^3}\left[\frac{3}{2}\frac{\partial^2 R_i}{\partial x^2}R_i^2 + 2\left(\frac{\partial R_i}{\partial x}\right)^2 R_i\right]. \tag{A.4}$$

The channel profile at the time of the maximum collapsing rate at the center, $\max\left(\frac{\partial R_i}{\partial t}\Big|_{x=0}\right)$ is used in the following estimation. If the shear rate and strain rate then is averaged over the cross-section and $-0.3\mathrm{L}/2 < \mathrm{x} < 0.3\mathrm{L}/2$ ($0.3\mathrm{L} \approx < \mathrm{X} >_{max}$), we obtained $|\overline{\epsilon_{rx}}| = 85.25(\frac{1}{s})$ and $|\overline{\epsilon_{xx}}| = 73.21(\frac{1}{s})$.

Appendix II: analytical solution of equation for collapsing channel

An analytical solution of Eq. (1) in a series form is available by using separation of variables [43].

$$R_i(\mathrm{x},t) = R_e - \frac{4(R_e-R_o)}{\pi}\sum_{k=0}^{\infty} exp\left[-\frac{(2k+1)^2\pi^2 C}{4\mathrm{x}_{max}^2}t\right]\sin\left[\frac{(2k+1)\pi}{2\mathrm{x}_{max}}\mathrm{x}\right] \tag{A.1}$$

Then, we have

$$R_i(0,t) = R_e - \frac{4(R_e-R_o)}{\pi}\sum_{k=0}^{\infty}\frac{(-1)^k}{2k+1}exp\left[-\frac{(2k+1)^2\pi^2 C}{4\mathrm{x}_{max}^2}t\right]. \tag{A.2}$$

Appendix III: generation of various DNA configurations

The globular, dumbbell, and half-dumbbell configurations are generated by following procedures. For the globular configuration, the position of the first bead is selected inside the channel. The position of the next bead is selected randomly among those in the equilibrium distance from the first bead on the condition that the nominal position is still inside the channel. The rest of the bead positions are selected in the same way as the second bead. The dumbbell configuration can be divided into three regions, two regions of globular configurations in both ends and one region of linear configuration in the middle. The globular configurations in the two regions are generated similarly as before. For the linear configuration in the middle, the positions of the next beads are randomly selected as before but the relative position in the channel axis direction, $x_{i+1} - x_i$, of all the beads have the same sign. i is the bead index. The half-dumbbell configurations are generated similarly. The fraction of chain in the linear form then represents the number of the bead generated in the linear configuration over the total bead number.

References

[1] J. Eid, A. Fehr, J. Gray, K. Luong, J. Lyle, G. Otto, P. Peluso, D. Rank, P. Baybayan, B. Bettman, Real-time DNA sequencing from single polymerase molecules, Science, 323 (2009) 133-138.

[2] S. Koren, M.C. Schatz, B.P. Walenz, J. Martin, J.T. Howard, G. Ganapathy, Z. Wang, D.A. Rasko, W.R. McCombie, E.D. Jarvis, A.M. Phillippy, Hybrid error correction and de novo assembly of single-molecule sequencing reads, Nat Biotechnol, 30 (2012) 692-+.

[3] E. Pennisi, Going Solid-State, Science, 336 (2012) 536-536.

[4] K.D. Dorfman, S.B. King, D.W. Olson, J.D.P. Thomas, D.R. Tree, Beyond Gel Electrophoresis: Microfluidic Separations, Fluorescence Burst Analysis, and DNA Stretching, Chem Rev, 113 (2013) 2584-2667.

[5] D.J. Mai, C. Brockman, C.M. Schroeder, Microfluidic systems for single DNA dynamics, Soft Matter, 8 (2012) 10560-10572.

[6] W. Reisner, J.N. Pedersen, R.H. Austin, DNA confinement in nanochannels: physics and biological applications, Rep Prog Phys, 75 (2012).

[7] X. Hu, P.E. Boukany, O.L. Hemminger, L.J. Lee, The Use of Microfluidics in Rheology, Macromol Mater Eng, 296 (2011) 308-320.

[8] T. Matsuoka, B.C. Kim, C. Moraes, M. Han, S. Takayama, Micro- and nanofluidic technologies for epigenetic profiling, Biomicrofluidics, 7 (2013).

[9] S.B. Smith, Y.J. Cui, C. Bustamante, Overstretching B-DNA: The elastic response of individual double-stranded and single-stranded DNA molecules, Science, 271 (1996) 795-799.

[10] C.H. Reccius, S.M. Stavis, J.T. Mannion, L.P. Walker, H.G. Craighead, Conformation, length, and speed measurements of electrodynamically stretched DNA in nanochannels, Biophys J, 95 (2008) 273-286.

[11] J. Tang, S.L. Levy, D.W. Trahan, J.J. Jones, H.G. Craighead, P.S. Doyle, Revisiting the Conformation and Dynamics of DNA in Slitlike Confinement, Macromolecules, 43 (2010) 7368-7377.

[12] W. Reisner, K.J. Morton, R. Riehn, Y.M. Wang, Z. Yu, M. Rosen, J.C. Sturm, S.Y. Chou, E. Frey, R.H. Austin, Statics and dynamics of single DNA molecules confined in nanochannels, Phys Rev Lett, 94 (2005) 196101.

[13] J.O. Tegenfeldt, C. Prinz, H. Cao, S. Chou, W.W. Reisner, R. Riehn, Y.M. Wang, E.C. Cox, J.C. Sturm, P. Silberzan, R.H. Austin, From the Cover: The dynamics of genomic-length DNA molecules in 100-nm channels, Proc Natl Acad Sci U S A, 101 (2004) 10979-10983.

[14] R. Chantiwas, S. Park, S.A. Soper, B.C. Kim, S. Takayama, V. Sunkara, H. Hwang, Y.K. Cho, Flexible fabrication and applications of polymer nanochannels and nanoslits, Chem Soc Rev, 40 (2011) 3677-3702.

[15] S. Mahshid, M.J. Ahamed, D. Berard, S. Amin, R. Sladek, S.R. Leslie, W. Reisner, Development of a platform for single cell genomics using convex lens-induced confinement, Lab on a Chip, 15 (2015) 3013-3020.

[16] C. Manneschi, P. Fanzio, T. Ala-Nissila, E. Angeli, L. Repetto, G. Firpo, U. Valbusa, Stretching of DNA confined in nanochannels with charged walls, Biomicrofluidics, 8 (2014) 064121.

[17] T. Matsuoka, B.C. Kim, J. Huang, N.J. Douville, M.D. Thouless, S. Takayama, Nanoscale squeezing in elastomeric nanochannels for single chromatin linearization, Nano Lett, 12 (2012) 6480-6484.

[18] D. Huh, K.L. Mills, X. Zhu, M.A. Burns, M.D. Thouless, S. Takayama, Tuneable elastomeric nanochannels for nanofluidic manipulation, Nat Mater, 6 (2007) 424-428.

[19] K.L. Mills, D. Huh, S. Takayama, M.D. Thouless, Instantaneous fabrication of arrays of normally closed, adjustable, and reversible nanochannels by tunnel cracking, Lab Chip, 10 (2010) 1627-1630.

[20] C. Freitag, C. Noble, J. Fritzsche, F. Persson, M. Reiter-Schad, A. Nilsson, A. Granéli, T. Ambjörnsson, K. Mir, J. Tegenfeldt, Visualizing the entire DNA from a chromosome in a single frame, Biomicrofluidics, 9 (2015) 044114.

[21] J. Sheats, J.G. Reifenberger, H. Cao, K.D. Dorfman, Measurements of DNA barcode label separations in nanochannels from time-series data, Biomicrofluidics, 9 (2015) 064119.

[22] P.T. Underhill, P.S. Doyle, Alternative spring force law for bead-spring chain models of the worm-like chain, Journal of Rheology (1978-present), 50 (2006) 513-529.

[23] R.D. Groot, P.B. Warren, Dissipative particle dynamics: Bridging the gap between atomistic and mesoscopic simulation, Journal of Chemical Physics, 107 (1997) 4423.

[24] S.M. Willemsen, H.C.J. Hoefsloot, P.D. Iedema, No-slip boundary condition in dissipative particle dynamics, International Journal of Modern Physics C, 11 (2000) 881-890.

[25] D.A. Fedosov, I.V. Pivkin, G.E. Karniadakis, Velocity limit in DPD simulations of wall-bounded flows, Journal of Computational Physics, 227 (2008) 2540-2559.

[26] L. Dai, J.R.C. van der Maarel, P.S. Doyle, Extended de Gennes Regime of DNA Confined in a Nanochannel, Macromolecules, 47 (2014) 2445-2450.

[27] D.R. Tree, Y.W. Wang, K.D. Dorfman, Modeling the relaxation time of DNA confined in a nanochannel, Biomicrofluidics, 7 (2013).

[28] Y. Wang, D.R. Tree, K.D. Dorfman, Simulation of DNA Extension in Nanochannels, Macromolecules, 44 (2011) 6594-6604.

[29] F. Meng, J. Huang, M.D. Thouless, The Collapse and Expansion of Liquid-Filled Elastic Channels and Cracks, J Appl Mech, 82 (2015) 1010091-10100911.

[30] W.F. Reinhart, D.R. Tree, K.D. Dorfman, Entropic depletion of DNA in triangular nanochannels, Biomicrofluidics, 7 (2013) 24102.

[31] C. Manneschi, E. Angeli, T. Ala-Nissila, L. Repetto, G. Firpo, U. Valbusa, Conformations of DNA in triangular nanochannels, Macromolecules, 46 (2013) 4198-4206.

[32] M.C. Cheng, A.T. Leske, T. Matsuoka, B.C. Kim, J. Lee, M.A. Burns, S. Takayama, J.S. Biteen, Super-resolution imaging of PDMS nanochannels by single-molecule micelle-assisted blink microscopy, J Phys Chem B, 117 (2013) 4406-4411.

[33] P.T. Underhill, P.S. Doyle, Alternative spring force law for bead-spring chain models of the

worm-like chain, J Rheol, 50 (2006) 513-529.

[34] P.T. Underhill, P.S. Doyle, Development of bead-spring polymer models using the constant extension ensemble, J Rheol, 49 (2005) 963-987.

[35] X.J. Fan, N. Phan-Thien, S. Chen, X.H. Wu, T.Y. Ng, Simulating flow of DNA suspension using dissipative particle dynamics, Phys Fluids, 18 (2006).

[36] W. Jiang, J. Huang, Y. Wang, M. Laradji, Hydrodynamic interaction in polymer solutions simulated with dissipative particle dynamics, The Journal of chemical physics, 126 (2007) 044901.

[37] J.A. Millan, M. Laradji, Cross-stream migration of driven polymer solutions in nanoscale channels: A numerical study with generalized dissipative particle dynamics, Macromolecules, 42 (2009) 803-810.

[38] I.V. Pivkin, G.E. Karniadakis, Controlling density fluctuations in wall-bounded dissipative particle dynamics systems, Phys Rev Lett, 96 (2006).

[39] K.D. Dorfman, S.B. King, D.W. Olson, J.D. Thomas, D.R. Tree, Beyond gel electrophoresis: microfluidic separations, fluorescence burst analysis, and DNA stretching, Chem Rev, 113 (2013) 2584-2667.

[40] K.M. Mohamed, A.A. Mohamad, A review of the development of hybrid atomistic–continuum methods for dense fluids, Microfluidics and Nanofluidics, 8 (2009) 283-302.

[41] R.M. Robertson, S. Laib, D.E. Smith, Diffusion of isolated DNA molecules: dependence on length and topology, Proceedings of the National Academy of Sciences, 103 (2006) 7310-7314.

[42] W. Reisner, K.J. Morton, R. Riehn, Y.M. Wang, Z. Yu, M. Rosen, J.C. Sturm, S.Y. Chou, E. Frey, R.H. Austin, Statics and dynamics of single DNA molecules confined in nanochannels, Physical Review Letters, 94 (2005) 196101.

[43] N. Lebedev, I. Skal'skaya, Y.S. Uflyand, Collection of Problems in Mathematical Physics, GITTL, Moscow, (1955).

This manuscript was accepted by Biomicrofluidics. Click here to see the version of record.

Table I. Comparisons for responses of various configurations according to periodic squeeze*

	Globular	**Dumbbell 0.1**	**Dumbbell 0.05**	**Half-dumbbell 0.2**
$< X >_{initial}/L$	0.058	0.099	0.068	0.107
$< X >_{max}/L$	0.13	0.24	0.15	0.20
τ^{**}**(sec)**	0.93	1.59	0.88	0.94

* The time interval is $T_{interval}$ =4(sec).

** τ is defined in Fig. 3(b).

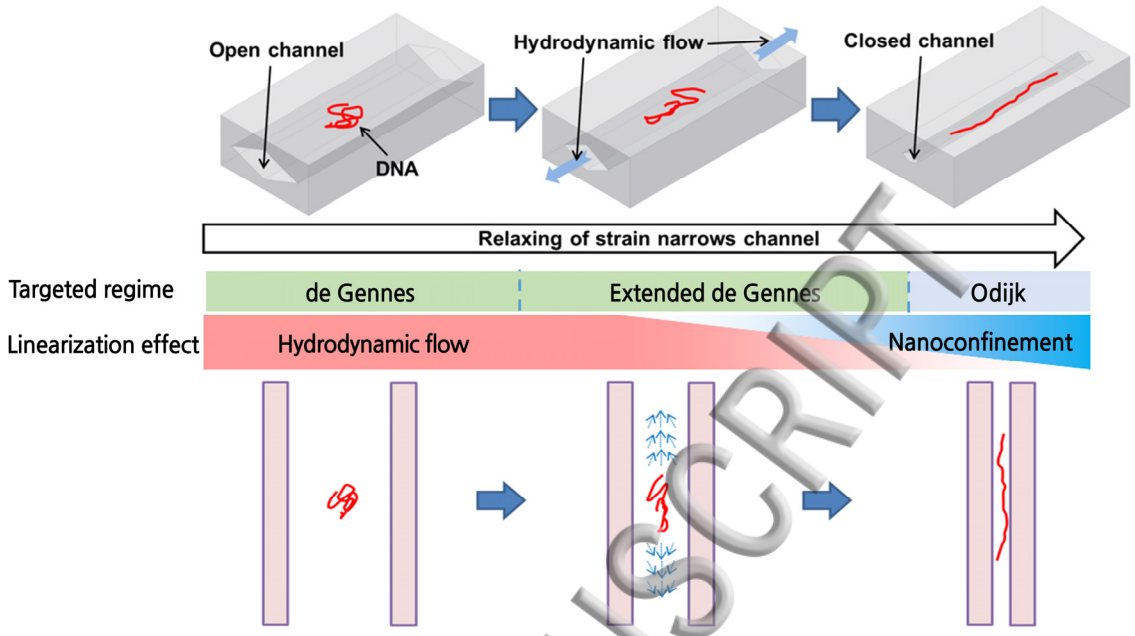

Figure 1 Schematic description of the experimental system. Channel narrowing create hydrodynamic effects and nanoconfinement effects to induce biopolymer linearization. The relative contribution of each effect changes with the diameter of the channel. The channel diameter effects follow biopolymer scaling regimes where D > 1547 nm puts λ-DNA is in the bulk state regime, 611 < D <1547 the de Gennes regime, 106<D<611 the extended de Gennes regime, 53<D<106 the crossover regime, and D < 53 the Odijk regime. Our simulation are of the de Gennes to extended de Gennes regimes.

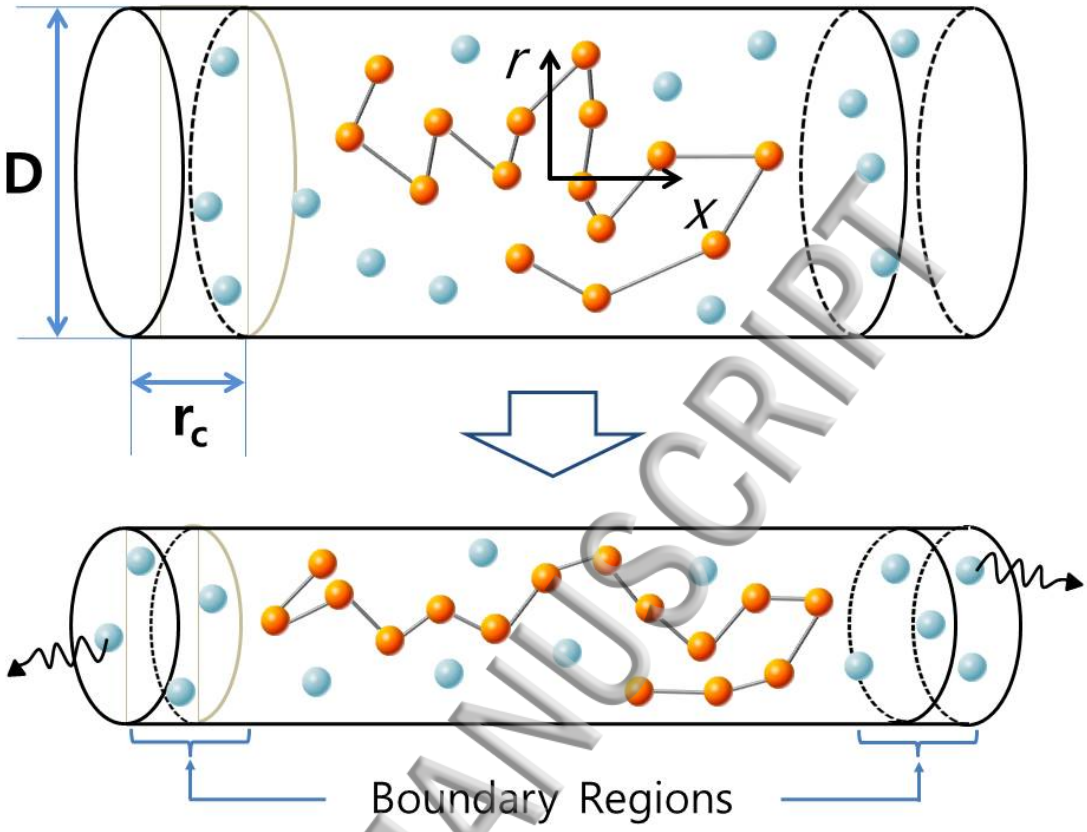

Figure 2 Validation of the simulation methods: (a) Schematic of the simulation performed. The number of water particles in the boundary regions is kept constant by removing randomly selected ones from the boundary.

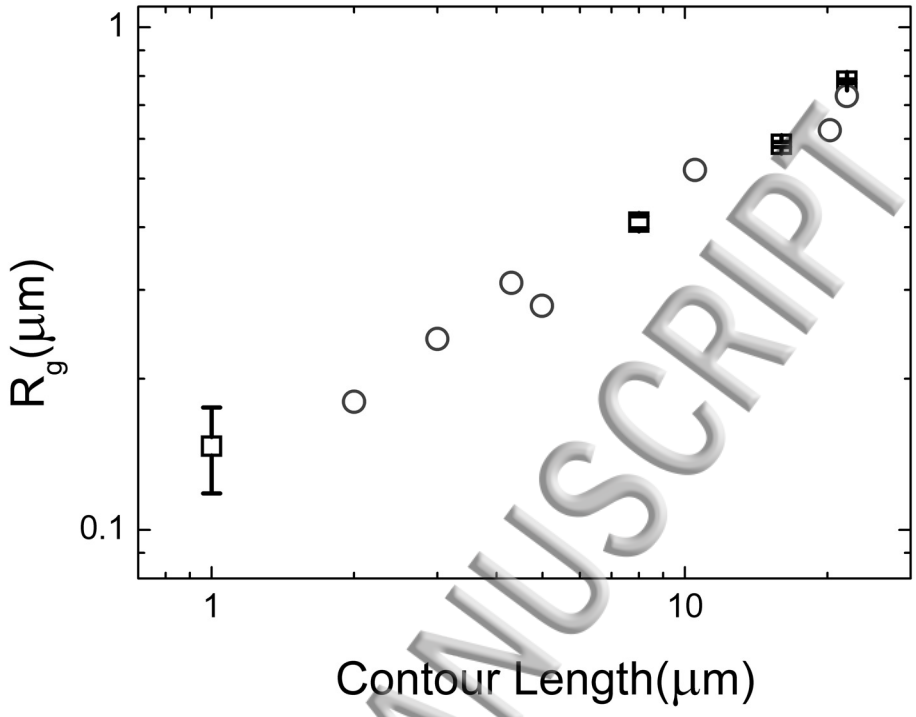

Figure 2 (b) Simulation results (square) compare well with experimental data (circle;[33]) for the radius of gyration (R_g) of DNA in bulk solution.

This manuscript was accepted by Biomicrofluidics. Click here to see the version of record.

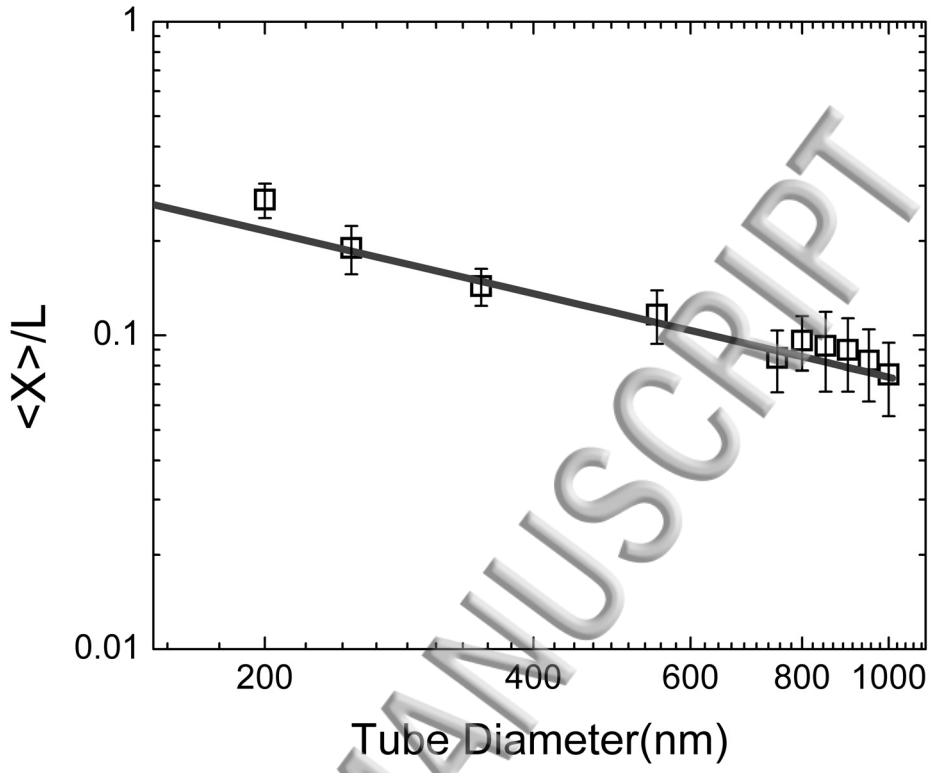

Figure 2 (c) Simulation results (square) compare well with theory (line) for the mean extension of DNA in confined geometries. The contour length is 22μm. The blob theory for the de Gennes regime is used where $\langle X \rangle / L = aD^{(\nu-1)/\nu}$ with ν=0.5877 [34]. The coefficient a=9.72 is obtained by fitting.

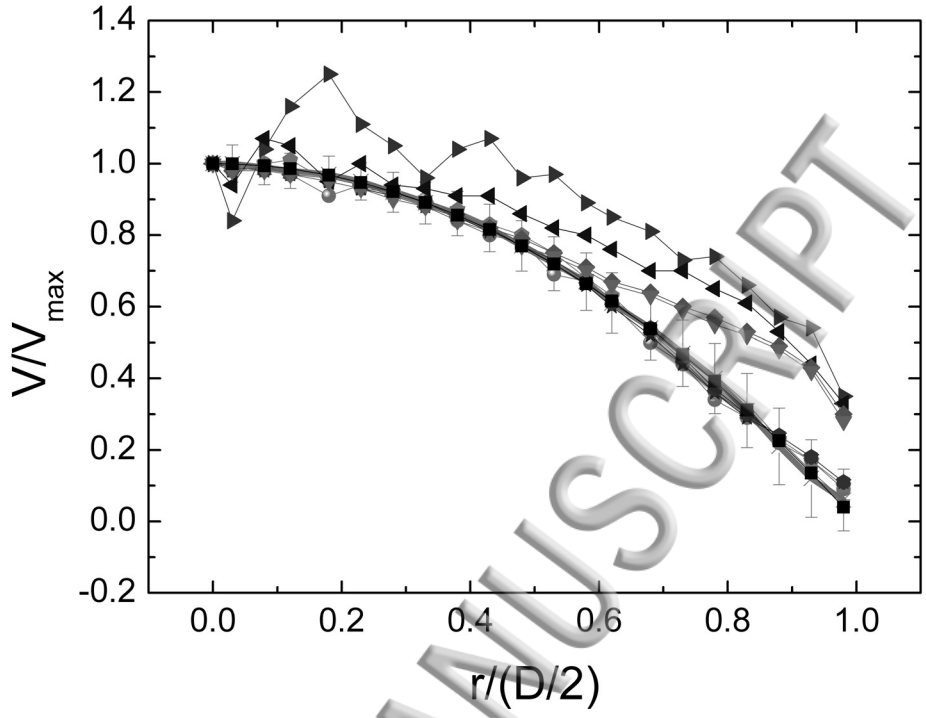

Figure 2 (d) Velocity profiles of flows driven by axial body forces within the cylindrical channels. Tube size relative to bead and maximum velocity [mm/sec] are varied as follows: 6.6, 5.2 for cross; 6.6, 53 for plus; 3.3, 0.036 for circle; 3.3, 0.069 for pentagon; 3.3, 1.4 for star; 3.3, 14 for hexagon; 1.7, 0.01 for right arrow; 1.7, 0.0025 for left arrow; 1.5, 0.62 for diamond; 1.5, 6.2 for down arrow. The line is for Poiseuille flow. All the error bars indicate the standard deviation.

This manuscript was accepted by Biomicrofluidics. Click here to see the version of record.

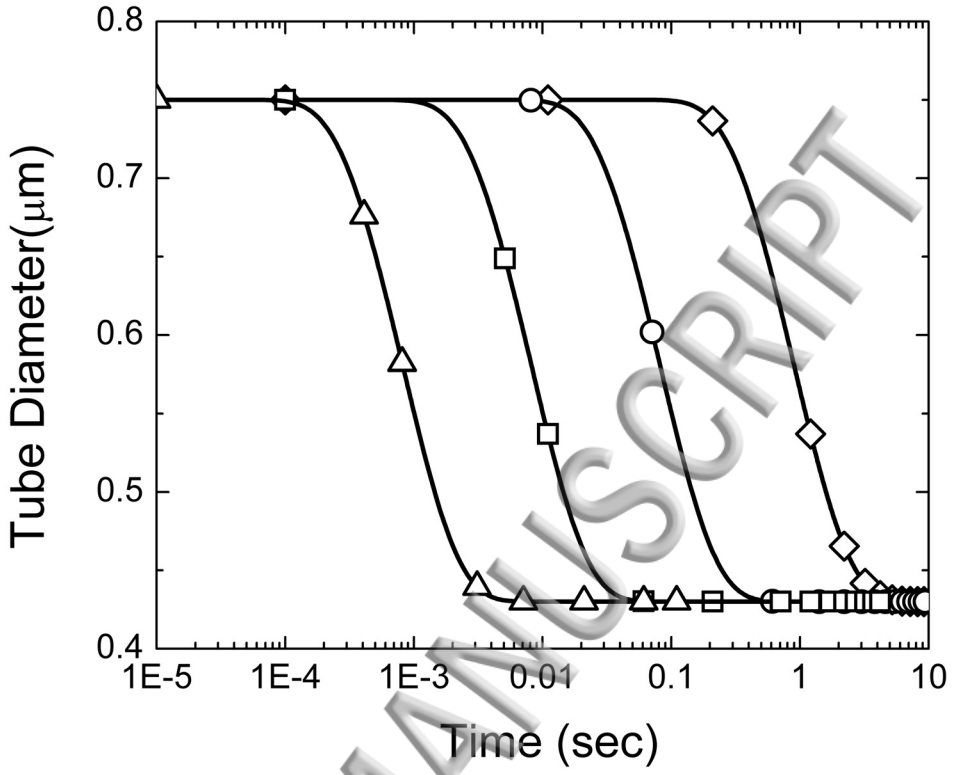

Figure 3 DNA over-stretches then recoils to new equilibrium length for when the channel diameter changes from 750 to 430 nm (L=22[μm]; 10 samples for (b) and 37 for (c,d)): (a) time history of the channel diameter at x=0 for $\mathbf{C}$ =10^4 (diamond), 10^5 (circle), 10^6 (square), and 10^7 (triangle). $\mathbf{C} \equiv (\boldsymbol{E}\boldsymbol{R}_{\boldsymbol{io}}^{\boldsymbol{2}}/\mathbf{24}\boldsymbol{\mu})(\boldsymbol{\rho}_{\boldsymbol{o}}^{\boldsymbol{2}}-\mathbf{1})/\boldsymbol{\rho}_{\boldsymbol{o}}^{\boldsymbol{2}}[\boldsymbol{\mu m}^{\boldsymbol{2}}/\boldsymbol{s}]$ is the collapse constant in Eq.(1).

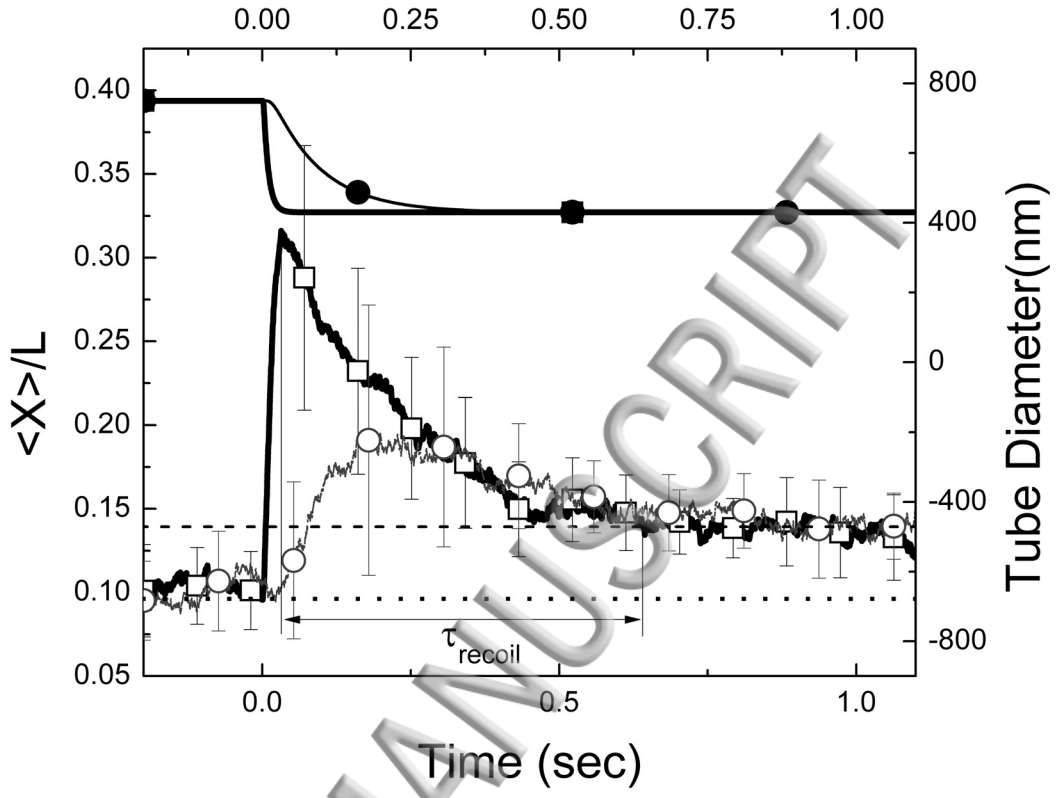

Figure 3 (b) ensemble-averaged channel-axial extension (X) of biopolymer normalized by its contour length (L) with channel for $\mathbf{C}$ =10^5 (open circle with thin line) and 10^6 (open square with thick line). time history of the channel diameter at x=0 for $\mathbf{C}$ =10^5 (filled circle with thin line) and 10^6 (filled square with thick line). The theoretical mean extensions are also given for the channel diameter of 430nm(dotted line) and 750nm(dashed line). The channel diameter results are the same as in (a). The vertical axis on the left is for the extension and the vertical axis on the right is for tube-diameter history.

This manuscript was accepted by Biomicrofluidics. Click here to see the version of record.

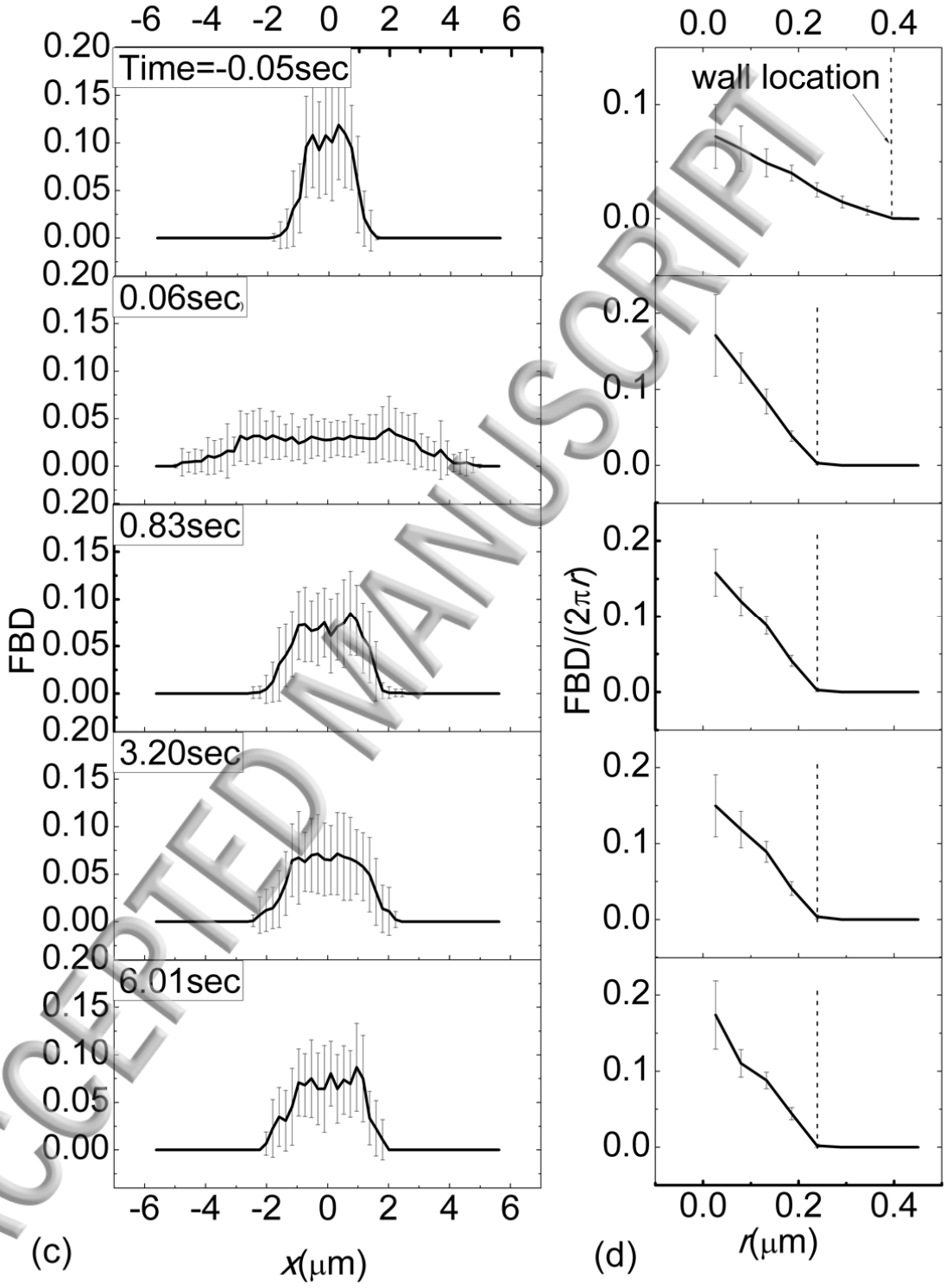

Figure 3 (c,d) time evolution of the fractional bead distribution (FBD) in the *x* and *r* coordinates for $\mathbf{C}$ =10^6. FBD is defined as the number of beads in a bin divided by total number of beads in chain. The bin size is 0.21[μm] × $\pi D^2/4$ for the distribution in *x*, and $(2\pi r)$0.053[μm] × L for the distribution in *r*.

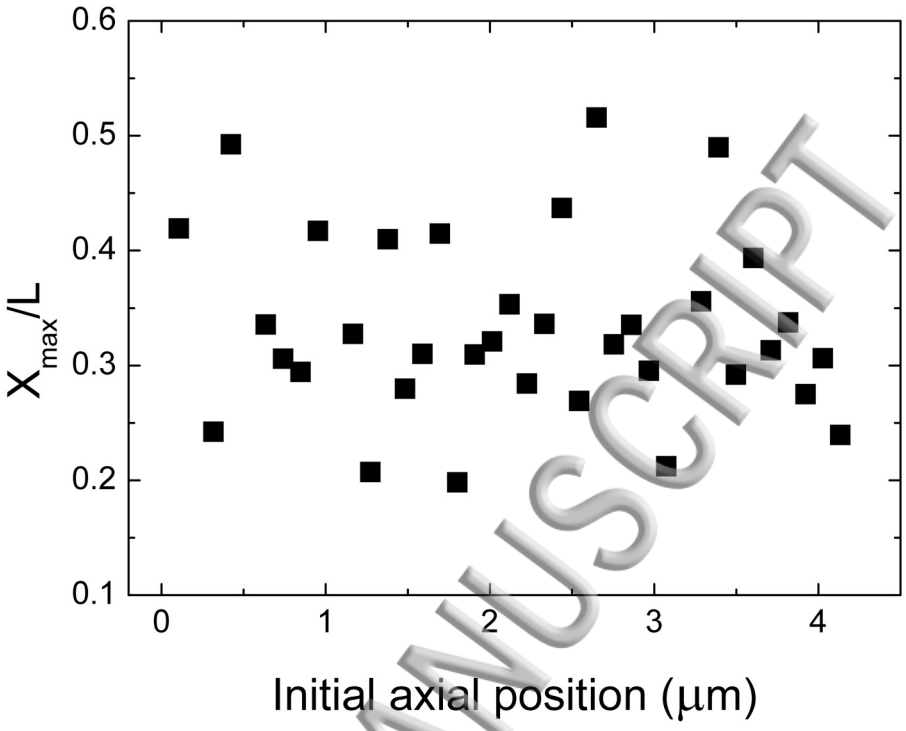

Figure 4 Simulation results for effect of CM position in channel-axial direction, starting state, and contour length: (a) maximum relative extension vs. initial CM position in channel-axial direction (L=22[μm]),

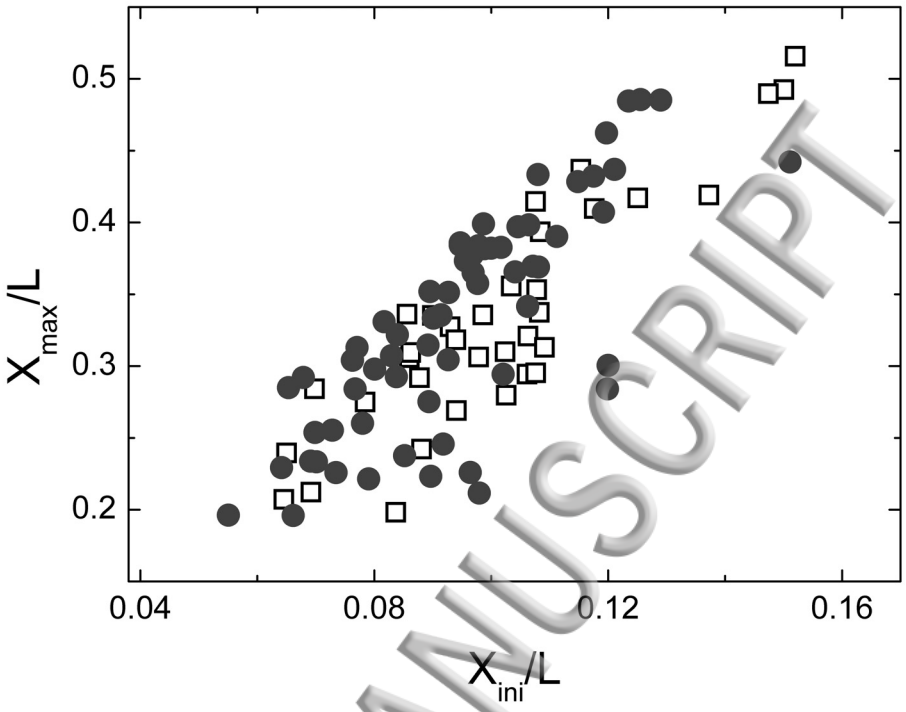

Figure 4 (b) maximum relative extension vs. initial relative extension for various initial positions (open square;L=22[μm]) and for various contour length(filled circle; L=10-80[μm]; Init. axial CM pos.=0.),

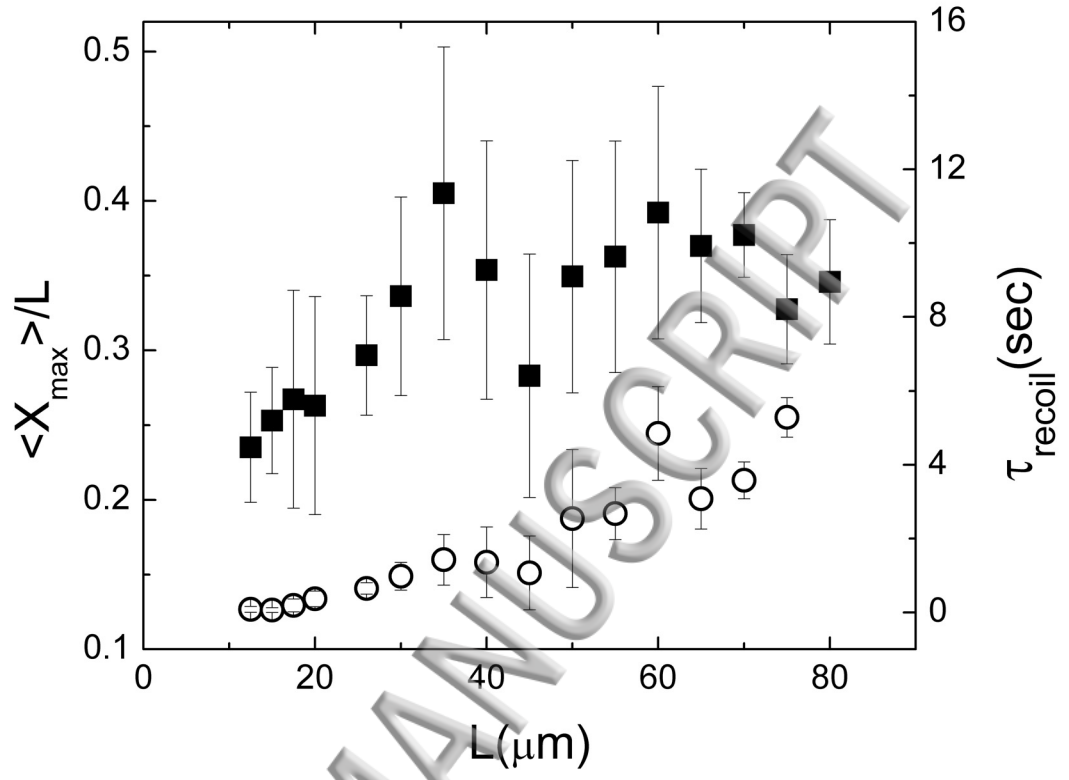

Figure 4 (c) ensemble-averaged maximum relative extension (square) and recoil time τ_{recoil} (circle) vs. contour length. τ_{recoil} is the period from the maximum extension to first arrival to equilibrium extension (See Fig. 4b.). The error bars indicate the standard deviation.

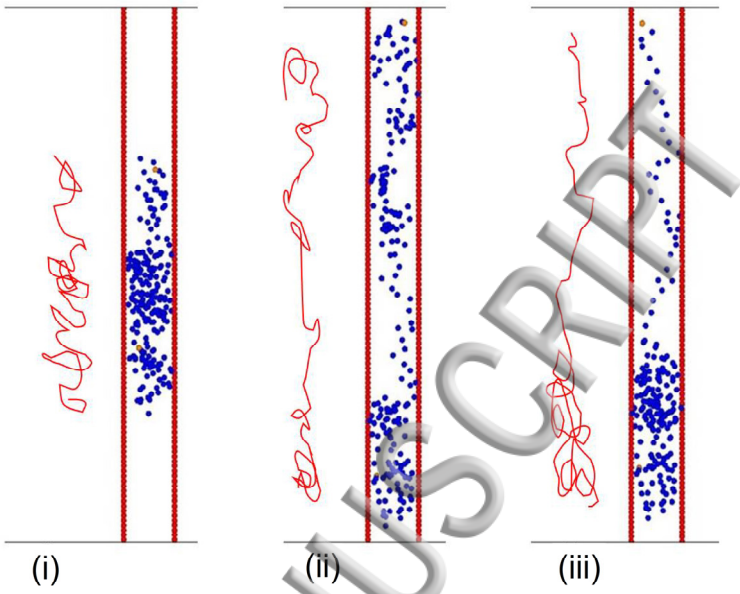

Figure 5 Simulation results for time evolution of DNA chains with various initial chain conformations in response to multiple narrow-widen operations (L=22[μm]; four evolution data are ensemble-averaged.) : (a) Three distinctive conformations that the chain can take: (i) globular, (ii) dumbbell, (iii) half-dumbbell.

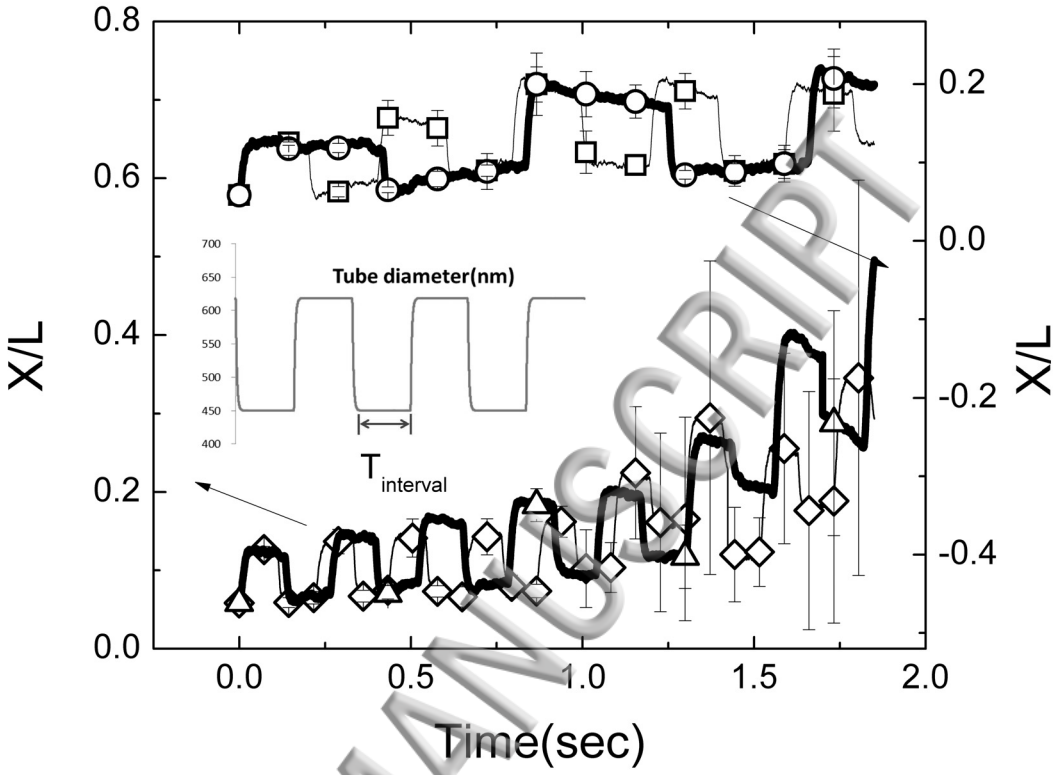

Figure 5 (b) time history of the tube diameter (inset) and *X/L* of the globular-initial-distribution case for time intervals, $T_{interval}$[sec]=0.07(diamond), 0.097(triangle), 0.1(square), and 0.32(circle).

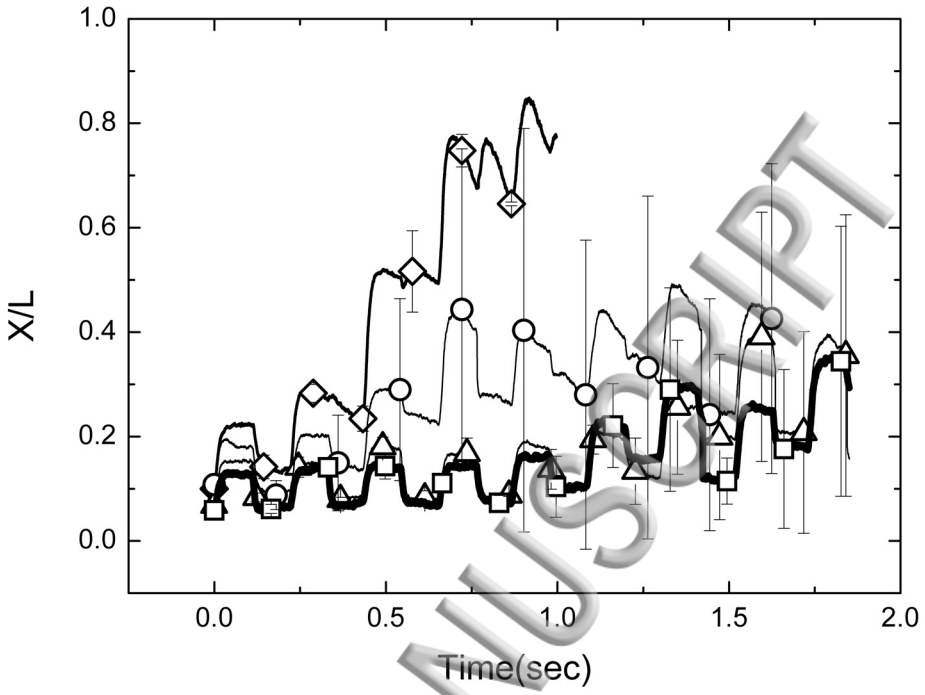

Figure 5 (c) time history of *X/L* for various chain conformations: dumbbell 0.1(diamond), dumbbell 0.05(triangle), half-dumbbell 0.2(circle), and globular(square). The numbers indicate the fractions of the linear distribution in the chain. $T_{interval}$[sec]=0.07

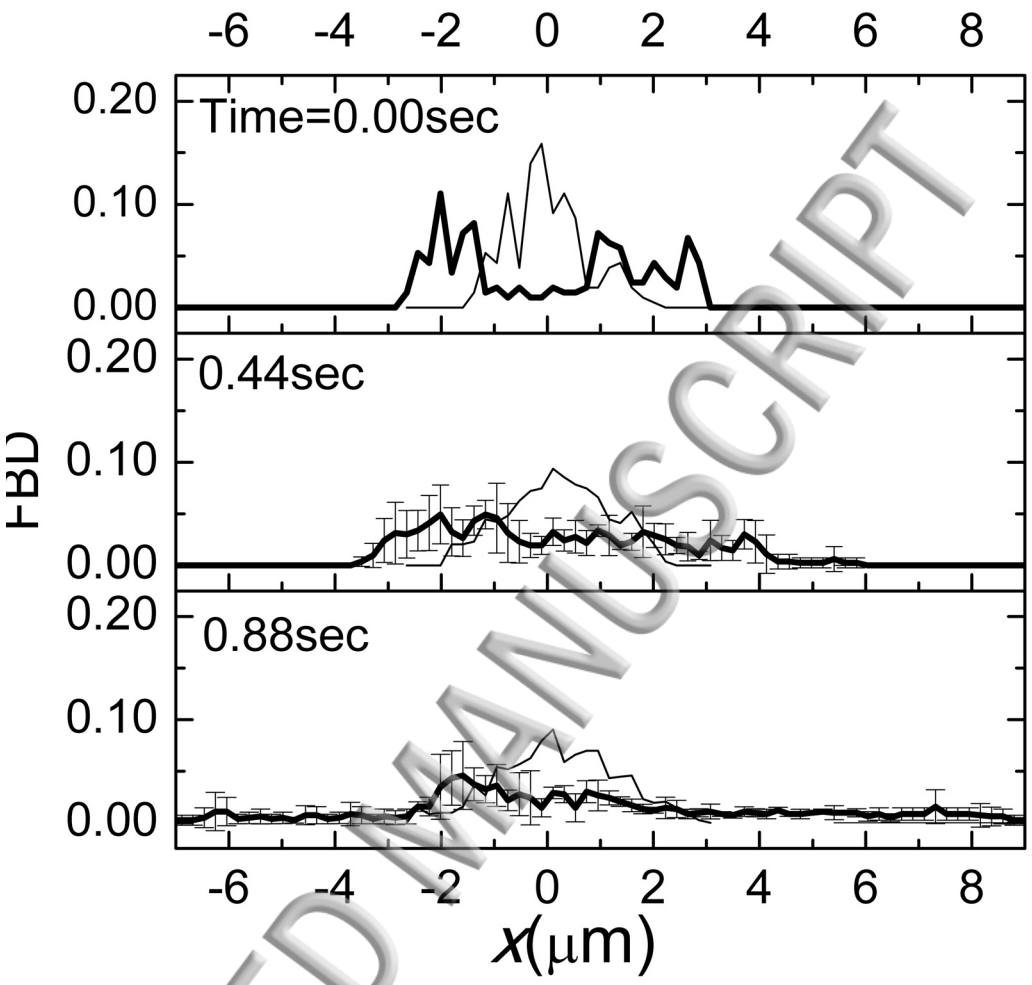

Figure 5 (d,e) Fractional distributions (FBD) of the dumbbell (d), globular (d), and half-dumbbell (e)

chains vs. time. FBD is defined in Fig. 3.

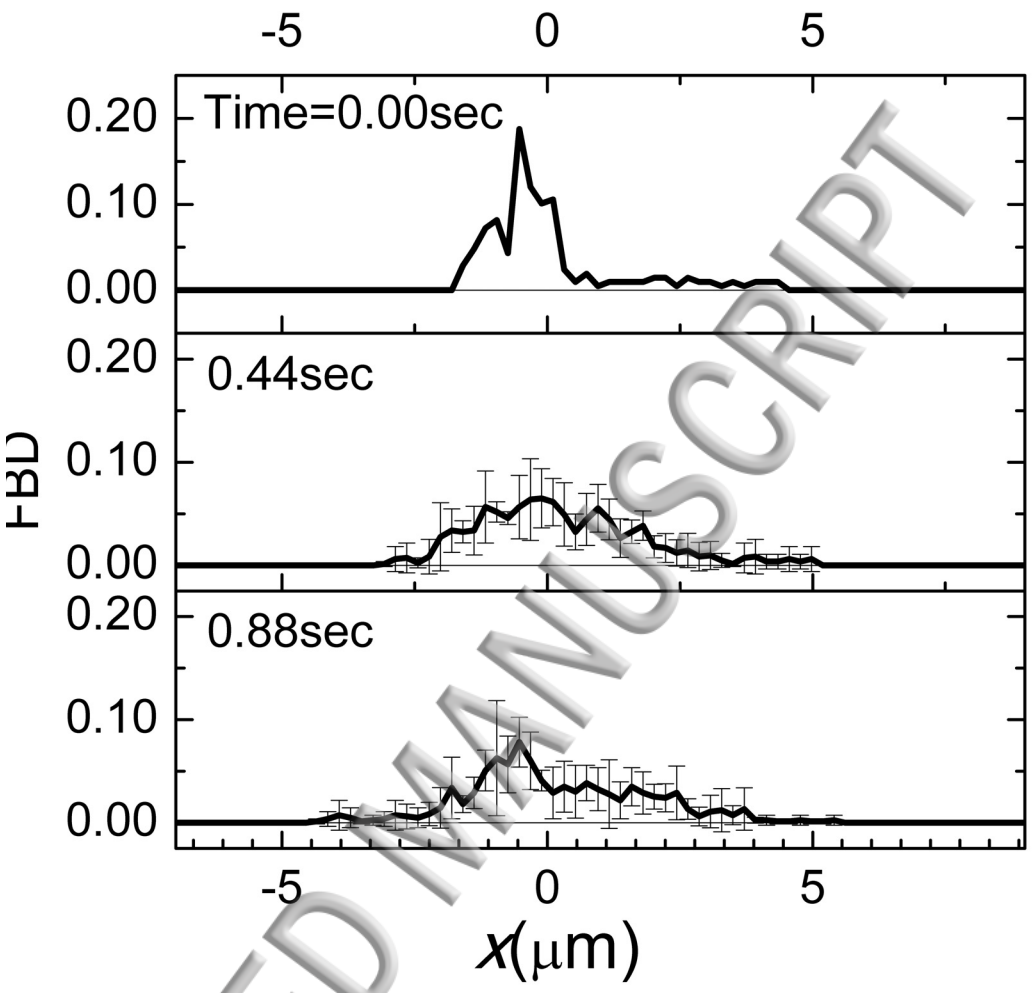

Figure 5 (continued from previous page)

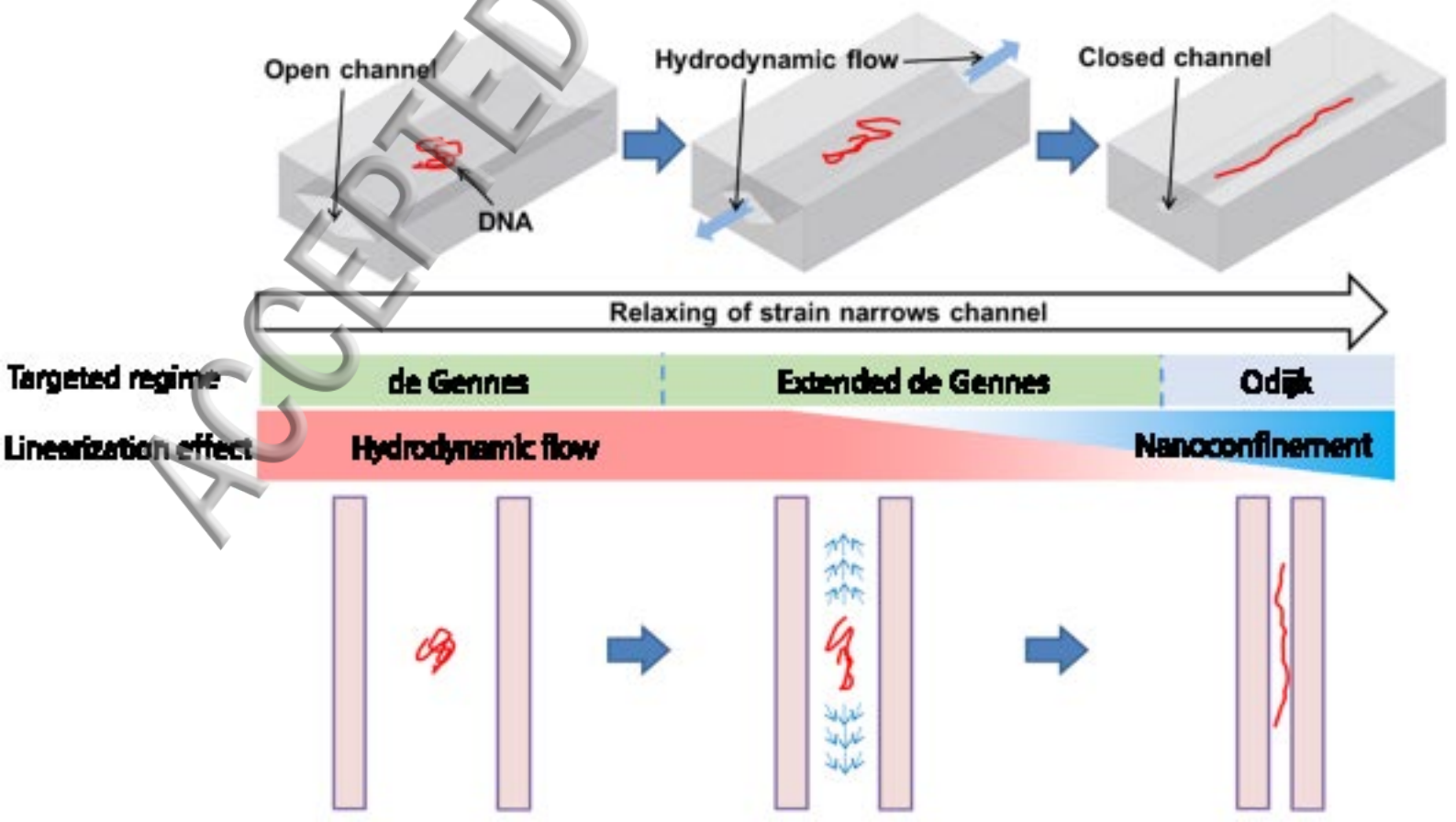
Open channel
DNA
Hydrodynamic flow
Closed channel
Relaxing of strain narrows channel
Targeted regime
de Gennes
Extended de Gennes
Odijk
Linearization effect
Hydrodynamic flow
Nanoconfinement